Bioconjugate Chemistry

Article

pubs.acs.org/bc

Fluorescent, Bioactive Protein Nanoparticles (Prodots) for Rapid, Improved Cellular Uptake

Inoka K. Deshapriya,[†] Bobbi S. Stromer,[†] Ajith Pattammattel,[†] Christina S. Kim,[†] Ramiro Iglesias-Bartolome,[‡] Laura Gonzalez-Fajardo,[§] Vyomesh Patel,[‡] J. Silvio Gutkind,[‡] Xiuling Lu,[§] and Challa V. Kumar*[,†]

[†]Department of Chemistry and Department of Molecular and Cell Biology, University of Connecticut, Storrs, Connecticut 06269-3060, United States

[‡]Oral and Pharyngeal Cancer Branch, National Institute of Dental and Craniofacial Research, National Institutes of Health, Bethesda, Maryland 20892-4340, United States

[§]Department of Pharmaceutics, School of Pharmacy, University of Connecticut, Storrs, Connecticut 06269-3092, United States

Supporting Information

ABSTRACT: A simple and effective method for synthesizing highly fluorescent, protein-based nanoparticles (Prodots) and their facile uptake into the cytoplasm of cells is described here. Prodots made from bovine serum albumin (nBSA), glucose oxidase (nGO), horseradish peroxidase (nHRP), catalase (nCatalase), and lipase (nLipase) were found to be 15−50 nm wide and have been characterized by gel electrophoresis, transmission electron microscopy (TEM), circular dichroism (CD), fluorescence spectroscopy, dynamic light scattering (DLS), and optical microscopic methods. Data showed that the secondary structure of the protein in Prodots is retained to a significant extent and specific activities of nGO, nHRP, nCatalase, and nLipase were 80%, 70%, 65%, and 50% of their respective unmodified enzyme activities. Calorimetric studies indicated that the denaturation temperatures of nGO and nBSA increased while those of other Prodots remained nearly unchanged, and accelerated storage half-lives of Prodots at 60 °C increased by 4- to 8-fold. Exposure of nGO and nBSA+ nGO to cells indicated rapid uptake within 1−3 h, accompanied by significant blebbing of the plasma membrane, but no uptake has been noted in the absence of nGO. The presence of nGO/glucose in the media facilitated the uptake, and hydrogen peroxide induced membrane permeability could be responsible for this rapid uptake of Prodots. In control studies, FITC alone did not enter the cell, BSA-FITC was not internalized even in the presence of nGO, and there has been no uptake of nBSA-FITC in the absence of nGO. These are the very first examples of very rapid cellular uptake of fluorescent nanoparticles into cells, particularly nanoparticles made from pure proteins. The current approach is a simple and efficient method for the preparation of bioactive, fluorescent protein nanoparticles of controllable size for cellular imaging, and cell uptake is under the control of two separate chemical triggers.

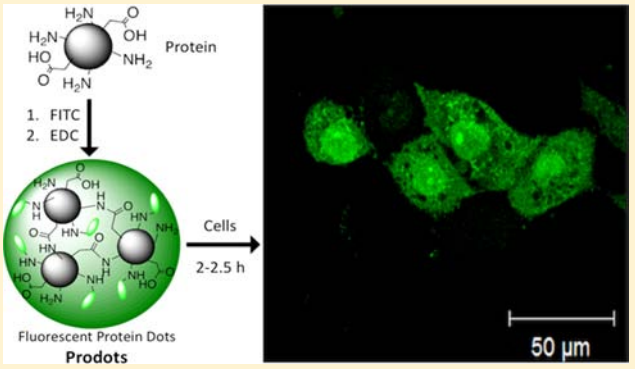

INTRODUCTION

Synthesis of protein nanoparticles (Prodots) that are highly fluorescent, stable, and versatile, and their rapid cellular uptake by cells is reported here. Currently, nanoparticles are extensively being used in a wide range of applications including biocatalysis,[1−3] drug delivery,[4−6] biosensing,[7−9] and bioimaging.[10−12] Nanoparticles are being tested for a variety of biological applications essentially due to their attractive properties and their amenability for surface modification.[13] However, many of them are toxic and their toxicity has not been fully evaluated. Protein-based nanoparticles that are stable, biocompatible, benign, and also strongly fluorescent for cellular imaging are highly desirable as alternatives.

Most prominent examples of nanoparticles used in cell imaging include but are not limited to semiconducting fluorescent nanocrystals or quantum dots (QD),[14] plasmonic nanoparticles such as gold and silver,[15] inorganic nanoparticles such as silicon,[16] and magnetic nanoparticles.[17] These nano-sized probes are designed to produce bright fluorescence detectable by optical methods. However, these probes require biocompatible surface coatings and appropriate modifications to reduce their toxicity and improve their fluorescence/solubility in aqueous media. Hence, nanoparticles synthesized

Received: May 17, 2014
Revised: January 18, 2015
Published: January 21, 2015

DOI: 10.1021/bc500621h
Bioconjugate Chem. 2015, 26, 396−404

that are biodegradable, nontoxic, and water-soluble, yet capable of emitting in a desired wavelength window, are urgently needed for imaging applications. Protein-based nanoparticles are advantageous over conventional quantum dots as these are more biocompatible and completely biodegradable, and a general approach to synthesizing such Prodots for imaging is described here.

Protein-based nanoparticles are generally prepared by freeze−drying,[18,19] supercritical fluid technology,[20] spray-drying,[21] desolvation,[22−24] and enzymatic cross-linking.[25] Most of these methods use organic solvents, drying, or dehydration, which may damage the delicate structures of proteins. Though supercritical fluid (SCF) methods use mild conditions, they mostly produce particles in the 1−10 μm size, with a wide size distribution.[26] α-Chymotrypsin nanoparticles, for example, prepared by SCF method were large (size ∼1 μm).[27,28] Alternative methods of Prodot synthesis with smaller particle sizes, higher retention of biological activities, and a fluorescent tag will be useful for imaging applications.

Controlling the size of Prodots is important, as this is one of the key factors governing their fate in biological systems.[29−33] Particles smaller than 10 nm are subjected to rapid renal clearance[34] while particles of 10−50 nm have the ability to distribute in intracellular and extracellular spaces without hindrance from the lymphatic system. Nuclear uptake of nanoparticles of sizes of up to 30 nm was suggested.[35] Particles of 100−200 nm are captured by the lymph nodes, while particles larger than 200 nm are concentrated in the spleen or taken up by phagocytic cells. On the other hand, larger particles are quickly captured and removed from the circulation.[36] The circulation time, therefore, depends on particle size. For example, 12 nm particles have 24.7 ± 4.0 h half-lives in mice, while 60 and 125 nm particles have half-lives of 16.6 ± 1.60 and 9.7 ± 0.8 h, respectively.[37] Therefore, controlling particle size is critical for biological applications. Prodots produced in this study are 10−50 nm wide, which is suitable for cellular uptake and imaging, and their size is under synthetic control.

An important issue with most nanoparticles is tracking their cellular uptake in real time. One approach has been to make fusion proteins with natural fluorescent proteins and subsequently prepare particles from these fusion products.[38] One drawback of this approach is the presence of the fluorescent protein in the nanoparticle, which may not be desirable for the intended application, and fusion may decrease particle stability or interfere with biological functioning of the protein/peptide or its folding. This approach, however, requires genetic engineering methodologies, and is not readily accessible to most chemical laboratories. Another approach has been to append fluorescent probes to the nanoparticles. For example, BSA nanoparticles (size, 100−150 nm) embedded with an infrared-absorbing dye were prepared by desolvation, cross-linking with glutaraldehyde, followed by solvent evaporation.[39] However, the use of organic solvents and glutaraldehyde may not be preferable for biological applications or for making nanoparticles that are intended to be biologically active after entering the cell. The current method does not use organic solvents or glutaraldehyde, but instead uses a general approach to produce highly fluorescent Prodots from a number of ordinary proteins and enzymes, under benign ambient conditions. Furthermore, these are nontoxic, biocompatible, and require no biophilic coatings to passivate hot spots; and they may be degraded into benign components by the normal biological mechanisms.[40−43]

Imaging with fluorescent Prodots reported here is advantageous in some ways, because specific chromophores of desired optical characteristics can be embedded or incorporated within the particles and the choice of chromophore is not restricted by limited access to naturally occurring fluorescent proteins.

A general approach is described here for the synthesis of fluorescein-labeled nanoparticles directly from several proteins, as a proof-of-concept. Specifically, fluorescently labeled nanoparticles of bovine serum albumin (nBSA), glucose oxidase (nGO), horseradish peroxidase (nHRP), catalase (nCatalase), and lipase (nLipase) are described here. Data indicated small size (<50 nm), narrow size distribution, high stability, high degree of retention of biological activity/structure, and rapid uptake by cells. The presence of nGO in the media facilitated rapid internalization of other Prodots for cell imaging.

RESULTS AND DISCUSSION

Synthesis of Protein Nanoparticles. In the current approach (Scheme 1), the amino groups of the lysine residues

Scheme 1. Prodot Synthesis by FITC Labeling Followed by EDC Cross-Linking of the Resulting Protein Clusters

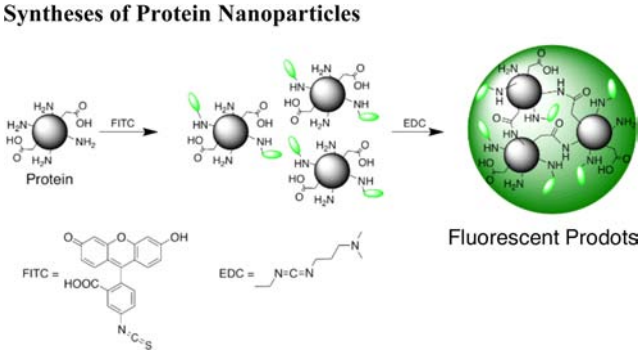

of proteins are coupled with FITC, followed by controlled aggregation of proteins and then cross-linking the protein units by EDC (Supporting Information (SI), Table S1). FITC labeling of proteins is known to induce clustering,[44,45] and here, we cross-link these clusters to form stable particles. Nanoparticle formation was monitored by dynamic light scattering (DLS), gel electrophoresis, and TEM, and the reaction conditions have been optimized to consume all the free protein while producing the desired particle size. The resulting Prodots were purified by dialysis or by centrifugation/filtration, and they have been thoroughly characterized by physical/biochemical methods before cellular imaging. Particle size was regulated by controlling the concentration of the dye, type of the dye, pH, and reaction time. For example, nBSA size varied from 8 to 50 nm, depending on the type of dye used (SI Figure S3).

Gel Electrophoresis. Agarose gel of nBSA obtained after 2 h of reaction time was imaged using UV excitation where the free FITC can be readily detected (Figure 1A, lane 6) and the nBSA-FITC band (lane 3) is distinctly visible. The free BSA (lane 1) migrated much farther (lane 1). Also, there was no free FITC in the nBSA-FITC lane. The same gel was also Coomassie stained to reveal the corresponding protein bands (Figure 1B), and nBSA-FITC (lane 3) did not indicate any free BSA (lane 2). Thus, nBSA has no detectable amounts of either FITC or BSA, which is also confirmed by other methods described below. The formation of nBSA was also confirmed by

DOI: 10.1021/bc500621h
Bioconjugate Chem. 2015, 26, 396−404

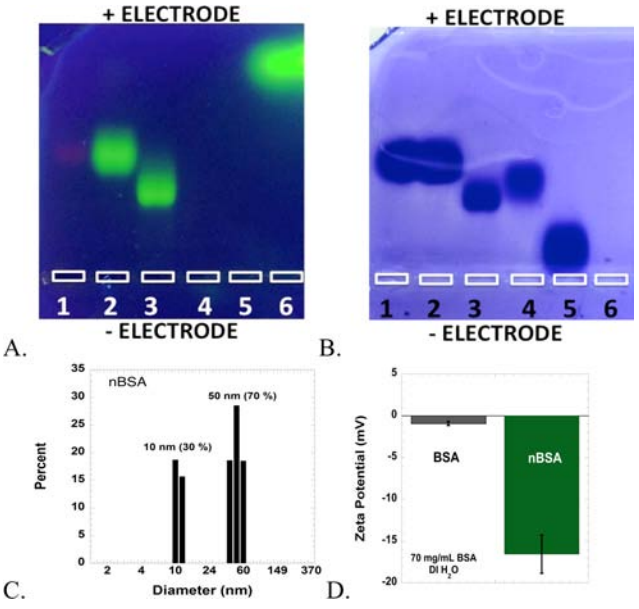

Figure 1. (A) Agarose gel (0.5%) of BSA (lane 1), BSA-FITC, (lane 2), nBSA-FITC (lane 3), GO (lane 4), nGO (lane 5), and FITC (lane 6). (B) The gel in (A) was Coomassie stained to reveal protein bands. (C) DLS plot of nBSA (diameters of 10 (30%) and 50 nm (70%)). (D) Zeta potential plot of BSA and nBSA.

DLS (Figure 1C) where the nBSA indicated a major particle diameter of 50 nm (70%) and a minor fraction of 10 nm (30%) particles, but no free BSA. This was also confirmed by the fact that the population of the 50 nm particle increased while that of the 10 nm particle decreased simultaneously as a function of reaction time (SI Figure S1). Thus, larger particles are produced from smaller ones as a function of reaction time, and this large particle size of nBSA (50 nm) explains its decreased mobility in the agarose gel (Figure 1A,B, lane 3).

Zeta potential studies of nBSA-FITC show a net negative charge of -18 ± 2 mV (Figure 1D), which is consistent with the consumption of the primary amine groups of BSA (-1.0 ± 0.2 mV, DI) after reaction with FITC. On the other hand, EDC cross-linking consumes equal numbers of amine and carboxyl groups and this reaction should not change the net charge. When taken together, nBSA particles are expected to have increased negative charge when compared to BSA, and this has been verified by zeta potential studies. Despite this increased negative charge, the larger size of nBSA impeded its mobility in the agarose gel. The sample was also examined by SDS PAGE (SI, Figure S2), which indicated extensive cross-linking of BSA and resulted in higher-order aggregates and only a trace amount of BSA. Thus, the agarose gel, SDS PAGE, DLS, and zeta potential data confirm the formation and purity of nBSA.

Using the above EDC cross-linking method, we also produced nGO (Figure 1A,B, lane 5), which moved far less than GO (lane 4). In contrast to the bimodal distribution of nBSA size, nGO indicated a single particle size of ~15 nm (100%). Similarly, Prodots were also made from HRP, lipase, and catalase, which consistently indicated reduced mobilities in agarose gels when compared to the respective unmodified proteins (data not shown). The isoelectric points of GO, BSA, and catalase are 4.2, 4.7, and 5.4, respectively. Therefore, they are all negatively charged at pH 7.0 (gel running buffer) and migrated toward the positive electrode. The corresponding Prodots were also negatively charged and migrated toward the positive electrode, but consistently to a lesser extent than their corresponding parents. The average pore size of the agarose gel (0.5% agarose) used here is ~450 nm[46] and all Prodots readily migrated through these pores. The reaction conditions were optimized to produce Prodots without any leftover free protein.

To further test the generality of the above approach with other dyes, we used Coumarin 540A (C540A) and pyrene-3-butyric acid (PBA), in place of FITC, and synthesized nBSA Prodots. The DLS (SI Figure S3) indicated the corresponding radii to be 10 nm for nBSA-C540A (100%) and 8 nm for nBSA-PBA (100%). Thus, the dye-mediated aggregation followed by EDC cross-linking of the proteins produced different particle sizes depending on the dye used as well as the reaction time. This general, simple, versatile approach of making fluorescent protein nanoparticles using a variety of dyes and proteins has significant advantages over reported methods.[47] It produced much smaller fluorescent Prodots whose size can be tuned systematically while carrying different fluorophores.

Sizes and Shapes of Prodots. Dynamic light scattering (DLS) and transmission electron microscopy (TEM) were used to examine the morphology, sizes, and shapes of Prodots. The hydrodynamic radii of nGO, nHRP, nLipase, and nCatalase were 8 (100%), 10 (98%), 25 (95%), and 25 (98%) nm, respectively (SI Figure S4). In contrast, enzyme particles prepared by various precipitation methods produced 5–50 μm particles, which are unsuitable for a number of biological applications.

The DLS data are supported by the TEM micrographs (Figure 2). Inset in each panel shows the expanded view of a single particle to clearly depict size and shape. Panel A shows nGO particles of size ~10 nm, whereas nHRP (panel B) had a diameter of ~20 nm and nLipase (panel C) a diameter of ~15 nm. These sizes are smaller than those noted in DLS, where the latter measures the hydrodynamic radius, which can be larger than the particle diameter. Drying of the samples on the TEM grid dehydrates the Prodots and shrinks them.

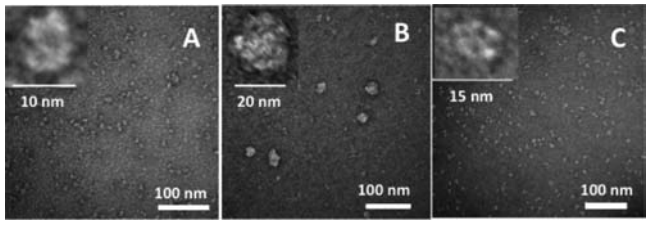

Figure 2. TEM images of protein nanoparticles (A) nGO, (B) nHRP, and (C) nLipase, with uranyl acetate staining. The bottom size bar represents 100 nm in all panels, and the inset shows the expanded view of one particle in each panel.

Spectral Measurements and Fluorescence Quenching Studies. Emission properties of Prodots were evaluated by fluorescence spectroscopy. As shown in SI Figure S5(A), fluorescence intensity of FITC bound to nanoparticles maintained more than 80% of FITC emission except in the case of nGO where the intensity decreased substantially. Emission spectra corresponded to that of FITC and changes observed in emission spectral shifts and intensities are presumably due to attachment of the fluorophore to the protein. This possibility was tested in fluorescence quenching studies with potassium iodide (KI). Iodide quenched FITC fluorescence with a Stern–Volmer constant (K_{sv}) of 16 M^{-1},

DOI: 10.1021/bc500621h
Bioconjugate Chem. 2015, 26, 396–404

whereas the corresponding K_{sv} value of nCatalase was significantly less (6 M^{-1}, SI Figure S5(B)). The decrease in K_{sv} indicates that the fluorophore in Prodots is protected by the protein matrix, likely due to its burial within Prodots. Therefore, Prodots are attractive for imaging studies since the fluorophore is also protected to a significant extent from quenchers in the environment by the protein matrix.

Protein Secondary Structure and Activity. The native structure of protein is vital for the retention of its biological activity. Therefore, the circular dichroism (CD) spectra of Prodots were compared with those of the corresponding free proteins to evaluate any distortions in the secondary structures during/after the formation of the particles.

The far-UV−CD spectra showed strong peaks at 192 nm and strong double minima at 209 and 222 nm (Figure 3A, SI Figure S6 and Table S2). The Prodot spectra were nearly superimposable with those of the corresponding free proteins, which indicated a significant retention of native-like secondary structures of the proteins present in Prodots.

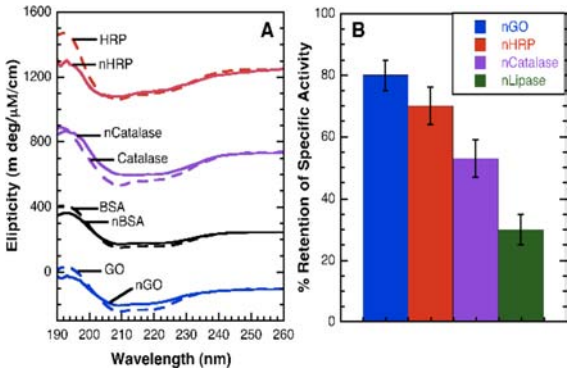

Figure 3. (A) Far-UV−CD spectra of Prodots (solid lines) and those of the corresponding parent proteins (dashed lines). (B) Percent retention of specific activities of Prodots with respect to those of the corresponding parent enzymes (100%).

In addition to the CD signals arising from the protein structure, we also observed induced CD (ICD) spectra for some of the Prodots, in the wavelength region corresponding to the fluorophore absorption band. For example, nBSA-FITC showed an intense ICD band at 550 nm (SI Figure S6B), which is due to the interaction of the fluorophore with the protein environment and its proximity to the asymmetric centers of the amino acid units of the protein.

The retention of protein secondary structure in Prodots suggested the possibility of retention of their biological activity. Enzymatic assays were performed and specific rates compared with those of the corresponding free enzymes, under similar conditions of pH, buffer, ionic strength, and temperature. For example, the catalytic activity of nGO was monitored by the oxidation of D-glucose to gluconic acid with ambient oxygen, and the production of hydrogen peroxide was measured by its reaction with guaiacol (substrate), catalyzed by HRP. Guaiacol oxidation resulted in a colored product whose formation was monitored by following its absorption at 470 nm as a function of time. Catalytic activity of nGO at 25 °C is close to that of GO (SI Figure S7). Extensive structure retention and facile diffusion of the substrate to the active site of the enzyme in the Prodots, therefore, are permitted even after the particle formation, which indicates that the active sites of enzymes in these particles are accessible for small molecules.

Specific activities of Prodots with respect to the corresponding unmodified enzymes are compared in Figure 3B, and nGO and nHRP retained significant activity while nLipase and nCatalase indicated a significant drop (SI Table S3). Note that the latter two formed much larger particles and larger particles would decrease the mass transfer to the active sites that are located in the interior of the particles. Thus, controlling particle size is critical in retaining significant activity. Next, we examined the stabilities of the particles for practical considerations, and lower conformational entropy of the protein within the confines of the Prodots may enhance Prodot thermal stability.

Thermal and Storage Stabilities of Prodots. Sufficient thermal and storage stabilities are essential for a wide use of protein nanoparticles. This metric was assessed by differential scanning calorimetry (DSC). DSC can provide a direct measure of the denaturation temperature (T_d), enthalpy (ΔH), heat capacity, and entropy changes. Both ΔH and T_d are obtained from DSC in a model independent manner, even when the denaturation is irreversible. Thermograms of Prodots, therefore, were quantified and compared with those of the corresponding parent proteins (SI Table S4). For example, T_d of nGO was 71 °C, far greater than that of GO (64 °C), T_d of nBSA (67 °C) was much greater than that of BSA (60 °C), but nHRP and nCatalase had T_d values of 85 and 64 °C, respectively, which are about the same as those of their parent proteins. Thus, some Prodots gained enhanced stability.

We further examined the thermal stability of nGO by heating to 60 °C for 5 min, followed by assessing their activities afer cooling the samples to room temperature. nGO showed retention of 75% of its original activity after the heat treatment, while GO lost ∼90% of its original activity under the same conditions (SI Figure S7). Thus, nGO was more stable when challenged with heat, when compared to that of GO.

In addition to temperature stability, another challenge with proteins is their poor storage stability, which requires storage at low temperatures, which is not convenient. Prodots are expected to have improved storage stabilities due to the encasement of proteins within the nanoparticles. To accelerate Prodot aging, we chose to store them at 60 °C, as a benchmark for stability (Na_2HPO_4 buffer pH 7.0), and examine activities. Aliquots of the samples were withdrawn, periodically, and specific activities measured at room temperature, and the time taken to decrease their original activity by 50% (storage half-life at 60 °C) has been calculated (SI Figure S8) from plots of specific activities of Prodots vs storage time at 60 °C.

Half-life of nGO increased to 30 min at 60 °C, when compared to that of GO (7 min), and nLipase half-life improved to 130 min when compared to that of lipase (15 min), while the half-life of nHRP remained the same as that of HRP (400 min, 60 °C). Improved half-lives at 60 °C suggest that storage stabilities at room temperature could be even better, an important attribute for practical considerations.

Cellular Imaging Studies. Our goal of producing stable, fluorescent, functional, biocompatible Prodots of controllable size has been aimed at testing their potential for cellular imaging. Cellular uptake and release studies with Prodots were performed using HN12 or A549 cells which have been extensively used for imaging.[35] Confocal microscopic imaging allowed us to test cellular uptake of Prodots (Figure 4).

Incubation of HN12 cells with nBSA-FITC for extended periods of time (132 min) did not show any detectable uptake (Figure 4). For example, the fluorescence micrograph recorded immediately after exposure of the HN12 cells to nBSA-FITC

DOI: 10.1021/bc500621h
Bioconjugate Chem. 2015, 26, 396−404

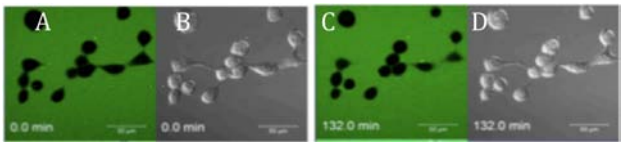

Figure 4. Lack of uptake of nBSA-FITC by HN12 cells even after 132 min of incubation. The fluorescence micrograph (A) and transmission micrograph (B) at 0 min of nBSA-FITC exposure to the cells (dark voids), and the corresponding images after 132 min of incubation (C and D).

(Figure 4A) was essentially the same as the one recorded after 132 min of incubation (Figure 4C), and the dark voids are the HN12 cells without the fluorophore; these matched well with the transmission micrographs (Figure 4B,D). Thus, we conclude that nBSA-FITC is unable to enter the cells on these time scales. We also obtained similar negative results when the HN12 cells were exposed to nLipase, nHRP, and nCatalase (0.3 mg/mL, 132 min, data not shown).

In contrast to the lack of uptake of nBSA-FITC by HN12 cells, incubation with nGO-FITC (0.3 mg/mL protein) indicated rapid uptake, and uptake has been visualized after washing the cells to remove unabsorbed nGO-FITC from the media and then imaged (Figure 5, SI Movie S1). Localization of

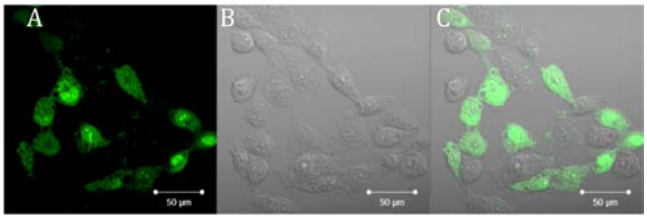

Figure 5. Facile uptake of nGO-FITC by HN12 cells after incubation for 4 h. Panel A is the fluorescence micrograph after 4 h, panel B is the corresponding transmission micrograph, while panel C is the superposition of the two. Scale bar represents 50 μm.

this fluorescent signal within the cells is clearly seen with bright spots in certain areas (Figure 5A, after 4 h). Superposition of the fluorescence (Figure 5A) and transmission (Figure 5B) images confirmed the uptake of nGO-FITC into the cells (Figure 5C).

Some cells were without any fluorescence signal, which indicated a failure in the uptake of nGO-FITC. This phenomenon of uneven cellular uptake is not unusual for cancer cells, since they are not a homogeneous population and some are different from the others.

In searching for a suitable explanation for the above observations where only nGO-FITC has been internalized but not the other Prodots, we tested the possibility of nGO-assisted uptake of Prodots. The HN12 cells were exposed to a mixture of nBSA-FITC (0.3 mg/mL) and unlabeled nGO (0.3 mg/mL) and they have been imaged for uptake. Surprisingly, there has been very rapid uptake of nBSA-FITC in less than an hour (Figure 6, SI Movie S2). For example, initially all the emission from the nBSA-FITC was located outside the cells (Figure 6A), whereas intense emission was noted from inside the cells in less than 132 min of incubation (Figure 6B, SI Movie S2). Overlay of the fluorescence images on the corresponding transmission images confirmed further that the emission is from within the cells (Figure 6 C,D). Thus, nBSA-

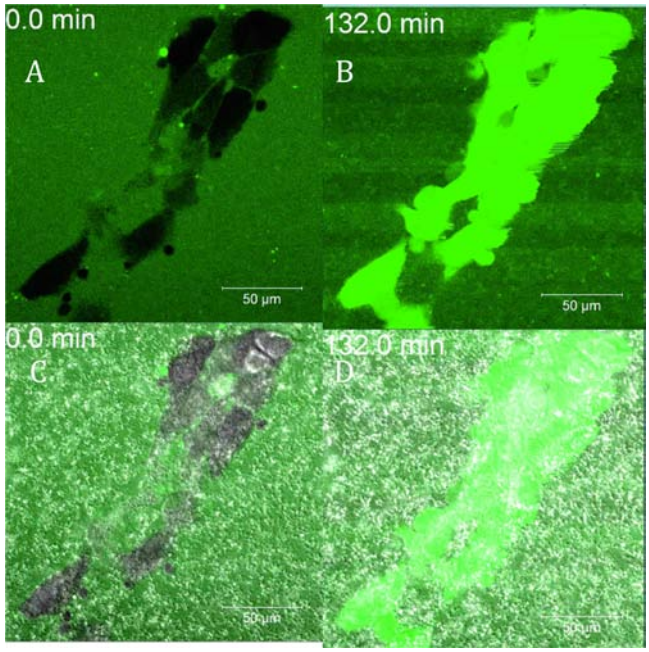

Figure 6. Rapid uptake of nBSA-FITC in the presence of unlabeled nGO by HN12 cells. Panels A and B are fluorescence images at 0 and 132 min, respectively, while panels C and D are the superpositions of the transmission and the fluorescence images at 0 and after 132 min of incubation, respectively.

FITC which did not enter the cells by themselves were now readily internalized through out the cytoplasm of the cells.

A likely explanation for this unexpected observation is that the culture media contained glucose, which is a substrate for nGO. The byproduct of glucose oxidation by nGO in the media would be hydrogen peroxide (H_2O_2), which is known to induce transient permeabilization of cell membranes and facilitate the uptake of certain ligands into the cells that are otherwise not internalized.[48,49]

In control experiments, we tested the uptake of BSA-FITC in the presence of unlabeled GO (SI Figure S9), even though nBSA-FITC did not have any free BSA-FITC. Incubation of BSA-FITC with A549 cells for 4 h did not indicate any uptake. In another control experiment, the direct uptake of FITC in the absence of GO was tested, even though nBSA-FITC did not have any free FITC. Again, FITC is not internalized by A549 cells even after incubation for 4 h (SI Figure S10), which confirms that the uptake noted in Figure 6 is due to the internalization of nBSA-FITC, not BSA-FITC, even in the presence of nGO, and there has been no direct uptake of FITC into the cells.

Since some control experiments were done with A549 cells but not HN12 cells, some explanation is essential. Both these cell lines have been used for a number of imaging studies. A recent review article[50] comparing the uptake of carbon nanotubes by a wide range of cell lines concluded that the uptake depended on the charge and the size of the nanotubes, but not the cell types. Thus, it appears logical that HN12 and A549 cells would behave in a similar manner toward our Prodots.

We analyzed the rates of internalization of nGO by live cells using time-lapse confocal microscopy and monitoring the emission intensity from particular cells as a function of time. Average fluorescence intensity from within the cells suddenly

DOI: 10.1021/bc500621h
Bioconjugate Chem. 2015, 26, 396−404

increased after 2−2.5 h of addition of nGO-FITC to the media, which suggested that the internalization of nGO has a lag phase (Figure 7A). The intensity after ∼200 min of incubation

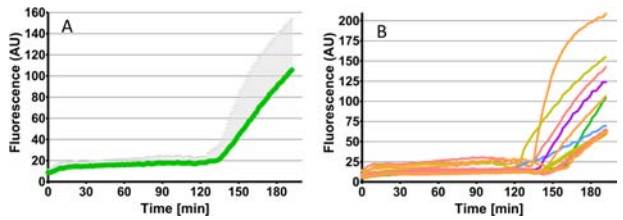

Figure 7. Quantification of time lapse, in vivo imaging of nGO internalization by HN12 cancer cells. (A) Average intracellular fluorescence intensity of 10 cells (green), and (B) fluorescence intensities from individual cells, AU: arbitrary units.

differed among different cells within the same culture, which is due to the differences in the uptake kinetics of individual cancer cells (Figure 7B). Interestingly, Prodot internalization was accompanied by significant vesicular out-pocketing of the plasma membrane (blebbing), which may be an indication of a transient permeabilization of the plasma membrane (SI Movie S1).

To further test the role of nGO in the internalization of Prodots, the HN12 cells were incubated for 2 h with nGO-FITC and dextran Texas Red (MW 10 000 Da), which is normally introduced into the cells by microinjection. Internalization of both dextran Texas Red and nGO occurred concurrently, and internalization is accompanied by significant blebbing, both of which indicated transient permeabilization by nGO-FITC and cellular uptake of dextran Texas Red (SI Movie S3).

The extent of cellular uptake of nGO-FITC and dextran Texas Red was quantified by measuring the amounts of emission from within two individual cells at the corresponding emission wavelengths and plotted as a function of incubation time (SI Figure S11). The growth of dextran Texas Red (red dots) followed that of nGO-FITC (green dots) in both the cells, even though the kinetics and extent of uptake were not identical.

In another study, the HN12 cells were also incubated with a mixture of alexa555-Transferrin and nGO-FITC for 3 h. The cells were then washed with fresh media to remove unbound dyes, and the release of alexa555-Transferrin (red dots) and nGO-FITC (green dots) from within the cells has been monitored as a function of time (SI Figure S12). These plots show the simultaneous release of both samples from within the cells to the outside media, but nGO-FITC has been released more rapidly (nearly complete in about an hour). Note that none of the cells are killed by Prodots, on these time scales, which is likely because of their high degree of biocompatibility.

These various uptakes as well as release studies clearly establish the utility of Prodots for imaging. In addition, the increased permeability of the plasma membrane due to nGO in the media facilitated the uptake of dextran Texas Red and alexa555-Transferrin, whose uptake kinetics were concurrent with the uptake of nGO into the cells. Thus, the data unequivocally demonstrate the utility of the Prodots for cellular uptake and imaging.

Recent studies on the kinetics of nanoparticle uptake by cells show that uptake of Tat peptide conjugated QDs (Tat-QD) by HeLa cells takes place slowly and complete accumulation is achieved only after 24 h.[51] In another study, AuNPs were conjugated with oligonucleotides to promote their uptake; these indicated faster cellular uptake than the particles without the oligonucleotide label.[52] Single-walled carbon nanotubes, graphene oxide, and carbon dots (C-dots) were used for cellular imaging, but their uptake kinetics have been much slower than those of Prodots.[53] For example, C-dots are taken up by human colon adenocarcinoma HT 29 cells only after overnight.[54] Semiconducting nanoparticles resist photobleaching when compared to most organic dyes, but cytotoxic effects of the semiconductor nanoparticles are a concern.[55] C-dots, on the other hand, are less toxic and photostable, but they show very slow kinetics of cellular internalization.[56]

In comparison to the existing nanoprobes, the Prodots described here have specific advantages, smaller size, higher stability, and long storage life, while retaining their biological activity to a significant extent, and these are promising alternatives as biocompatible tools for imaging. Prodot surfaces could be decorated with affinity ligands that are capable of cell-specific delivery with improved uptake efficiency for monitoring particle trafficking and localization.[57] Current studies clearly demonstrate the potential of Prodots as imaging agents and alternatives to other nanoparticles.

■ CONCLUSIONS

A new, simple, and effective approach was developed for the first time to synthesize purely protein-based nanoparticles with a size range of 10−50 nm, which falls under the expected size range for cellular imaging. Due to their inherent biocompatibility and biodegradability, together with low toxicity, Prodots are positioned as multitasking bright materials compared to any other existing nanomaterials, such as QDs or other NPs. In addition to their preserved biological activity, Prodots showed improved half-life and enhanced thermal stabilities and these unique properties may facilitate their use in imaging. Most importantly, the fact that Prodots are rapidly internalized into cells in the presence of nGO and glucose without causing cell death indicates certain advantages of using them for live cell imaging. Thus, the NP uptake was observed only in the presence of nGO and glucose while there has been no uptake without these. Thus, controlled uptake with a dual trigger has been demonstrated here.

■ EXPERIMENTAL SECTION

Proteins and Chemicals. Glucose oxidase (GO, *Aspergillus niger*), horseradish peroxidase (HRP, *Amoracia rusticana*), lipase (*Candida rugosa*), sodium phosphate (Na_2HPO_4), fluorescein isothiocyanate (FITC), and 1-ethyl-3-(-3-dimethylaminopropyl) carbodiimide (EDC), pyrene-3-butyric acid (PBA), and coumarin 540A (C540A) were purchased from Sigma (St. Louis, MO). Bovine serum albumin (BSA) and Catalase were purchased from US Biologicals (Salem, MA) and Worthington Biochemical Co., (Lakewood, NJ), respectively.

Synthesis of Prodots. Protein solutions were prepared by stirring protein (3 mg/mL) in 0.1 M carbonate/bicarbonate buffer, pH adjusted to 9.0. A solution of FITC (0.075 mg/mL, 0.2 mM) in DMSO was added to the protein solution and stirred for 1.3 h. The pH of the resulting solutions was adjusted depending on the pI of the protein (SI Table S1). Finally, a solution of EDC (10 mg/mL, 52 mM) was added to the protein/fluorescein solution and stirred overnight. The nBSA particle size increased with reaction time (SI Method S1.1,

DOI: 10.1021/bc500621h
Bioconjugate Chem. 2015, 26, 396−404

Figure S1) and particle size has been conveniently controlled a by adjusting the reaction time. Samples were dialyzed (25 kDa cutoff membranes, 10 mM Na_2HPO_4 pH 6.0) or purified by ultrafiltration until the filtrates were free of FITC. Samples were routinely analyzed by agarose gel electrophoresis and SDS PAGE (SI Method S1.2, Figure S2) for purity.

Dynamic Light Scattering (DLS) and Zeta Potential Studies. Hydrodynamic radii were measured by means of photon correlation spectroscopy with Precision Detectors (Varian Inc.), CoolBatch+ dynamic light scattering apparatus with a 5 × 5 mm^2 square cuvette, 658 nm excitation laser source with a 90° geometry. Data collection was done at 26 °C, for 1 s, 5 repetitions, with 60 accumulations after equilibrating the sample for 300 s. Prodots and their corresponding proteins (0.2 mg/mL in 10 mM Na_2HPO_4, pH 7) were routinely filtered with a 0.2 μm filter (PVDF, 13 mm, Fisher). Precision Elucidate v 1.1.0.9 and Precision Deconvolve v 5.5 were used to collect and process the data, respectively. Zeta potentials were measured on a Brookhaven Instruments Zeta Plus analyzer using the software from the manufacturer, as described before.[58]

Transmission Electron Microscopy (TEM). The nanoparticle solution (0.2 mg/mL) was applied to a carbon-coated Cu grid (400-mesh) after treating the grid with a plasma cleaner (Harrick PDC-32G). Aliquots of 3 μL were incubated on the grid for 60 s, blotted with filter paper (Whatman #4), and stained with 3 μL of 1% uranyl acetate for 30 s followed by blotting. After an hour of drying, the grids were imaged using a FEI Tecnai Spirit TEM with an operating voltage of 80 kV and a digital camera.

Spectral Measurements. Absorption spectra were run on HP 8450 diode array spectrophotometer (Varian Inc., Santa Clara, CA) and fluorescence spectra were recorded on a home-built instrument interfaced with a Macintosh Mini operated by in-house software. To keep the absorbance less than 1, a short path length cuvette (1 mm × 10 mm) was used, samples were excited at 495 nm, and all spectra were normalized to the same intensity for comparison.

Fluorescence Quenching Studies. Prodots (nCatalase) were titrated with increasing concentrations of potassium iodide (KI) and FITC emission at 525 nm (exciting at 490 nm) monitored. Stern−Volmer plots were constructed and the quenching constants (K_{sv}) determined using the equation below, where I_0 is the fluorescence in the absence of the quencher and I the intensity in the presence of the quencher at concentration [Q].

$$I_0/I = 1 + K_{sv}[Q]$$

Activity Studies and Half-Lives of Nanoparticles at 60 °C. Enzymatic activities of Prodots and the unmodified enzymes were determined by reported methods (SI, Method S1.3), and specific activities determined from the initial rates.[59−61] Time taken to reduce the enzymatic activity by half of its original activity (half-life) was estimated by measuring their activities at room temperature after heating at 60 °C for increasing lengths of time. Half-life was obtained by plotting specific activities of samples measured at room temperature, as a function of incubation time at 60 °C.

Cellular Imaging Studies. HN12 oral cancer cells were grown onto glass bottom microwell plates (#1.5 glass, MatTek Corporation), washed using DMEM without Phenol Red and FBS (Invitrogen) and incubated in the same media with 0.3 mg/mL of Prodots (SI Method S1.4). In some studies, A549 cells were used, instead (SI Method S1.5). Live cell imaging was done at 37 °C in 5% CO_2 atmosphere (HN12 cells) using an inverted Zeiss LSM 700 confocal microscope, with Zen software 2010 (Carl Zeiss). For measuring the uptake and release kinetic measurements, a region of interest (ROI) was drawn around each cell and the average fluorescence intensity recorded in particular channels as a function of time.

Differential Scanning Calorimetry. Thermal denaturation of Prodots was performed using Nano II differential scanning calorimeter (DSC) (model 6100, CSC, Utah). Unmodified protein and Prodot solutions (10 mM Na_2HPO_4 buffer pH 7.2) were scanned. The specific heat of the sample was measured as a function of temperature with respect to a reference cell, from 20 to 100 °C, at a scan rate of 2 °C/min. Excess molar heat capacities were calculated using molar masses of corresponding proteins. Model independent parameters such as peak transition temperature (T_m), the temperature where the denaturation begins, and $\Delta H_{denaturation}$ (integral $C_p dT$) were extracted from the DSC data.

■ ASSOCIATED CONTENT

Ⓢ Supporting Information

Synthesis conditions, protocols, DLS profiles of Prodots, fluorescence quenching data, induced-CD data, far-UV CD data, half-lives, specific activities, DSC data of Prodots, and movies and plots of their cellular uptake and release. This material is available free of charge via the Internet at http://pubs.acs.org.

■ AUTHOR INFORMATION

Corresponding Author

*E-mail: challa.kumar@uconn.edu. Phone: 860-486-3213. Fax: 860-486-2981.

Notes

The authors declare no competing financial interest.

■ ACKNOWLEDGMENTS

This publication is in fond memory of late Professor Nicholas J. Turro of Columbia University. Authors (C.V.K. and I.K.D.) are grateful for the generous financial support of this work by the NSF EAGER award (DMR-1441879).

■ ABBREVIATIONS

Prodots, protein nanoparticles; NP, nanoparticles; QD, quantum dots; CD, circular dichroism; TEM, transmission electron microscopy; DLS, dynamic light scattering; PNPA, *para*-nitrophenyl acetate; C-Dots, carbon dots

■ REFERENCES

(1) Yang, H.-H., Zhang, S.-Q., Chen, X.-L., Zhuang, Z.-X., Xu, J.-G., and Wang, X.-R. (2004) Magnetite-containing spherical silica nanoparticles for biocatalysis and bioseparations. *Anal. Chem. 76*, 1316−1321.

(2) Bornscheuer, U. T. (2003) Immobilizing enzymes: how to create more suitable biocatalysts. *Angew. Chem., Int. Ed. 42*, 3336−3337.

(3) Gao, L., Zhuang, J., Nie, L., Zhang, J., Zhang, Y., Gu, N., Wang, T., Feng, J., Yang, D., Perrett, S., et al. (2007) Intrinsic peroxidase-like activity of ferromagnetic nanoparticles. *Nat. Nanotechnol. 2*, 577−583.

(4) Kumar, A., Chen, F., Mozhi, A., Zhang, X., Zhao, Y., Xue, X., Hao, Y., Zhang, X., Wang, P. C., and Liang, X.-J. (2013) Innovative pharmaceutical development based on unique properties of nanoscale delivery formulation. *Nanoscale 5*, 8307−8325.

DOI: 10.1021/bc500621h
Bioconjugate Chem. 2015, 26, 396−404

(5) Dobson, J. (2006) Magnetic nanoparticles for drug delivery. *Drug Dev. Res. 67*, 55−60.
(6) Cho, K., Wang, X., Nie, S., Chen, Z. G., and Shin, D. M. (2008) Therapeutic nanoparticles for drug delivery in cancer. *Clin. Cancer Res. 14*, 1310−1316.
(7) Slowing, I. I., Trewyn, B. G., Giri, S., and Lin, V. S. Y. (2007) Mesoporous silica nanoparticles for drug delivery and biosensing applications. *Adv. Funct. Mater. 17*, 1225−1236.
(8) Selvan, S. T., Tan, T. T. Y., Yi, D. K., and Jana, N. R. (2009) Functional and multifunctional nanoparticles for bioimaging and biosensing. *Langmuir 26*, 11631−11641.
(9) Sannomiya, T., and Vörös, J. (2011) Single plasmonic nanoparticles for biosensing. *Trends Biotechnol. 29*, 343−351.
(10) Bertorelle, F., Wilhelm, C., Roger, J., Gazeau, F., Ménager, C., and Cabuil, V. (2006) Fluorescence-modified superparamagnetic nanoparticles: intracellular uptake and use in cellular imaging. *Langmuir 22*, 5385−5391.
(11) Thurn, K., Brown, E., Wu, A., Vogt, S., Lai, B., Maser, J., Paunesku, T., and Woloschak, G. (2007) Nanoparticles for applications in cellular imaging. *Nanoscale Res. Lett. 2*, 430−441.
(12) Alkilany, A. M., Nagaria, P. K., Hexel, C. R., Shaw, T. J., Murphy, C. J., and Wyatt, M. D. (2009) Cellular uptake and cytotoxicity of gold nanorods: molecular origin of cytotoxicity and surface effects. *Small 5*, 701−708.
(13) Maham, A., Tang, Z., Wu, H., Wang, J., and Lin, Y. (2009) Protein-based nanomedicine platforms for drug delivery. *Small 5*, 1706−1721.
(14) Bradburne, C. E., Delehanty, J. B., Boeneman Gemmill, K., Mei, B. C., Mattoussi, H., Susumu, K., Blanco-Canosa, J. B., Dawson, P. E., and Medintz, I. L. (2013) Cytotoxicity of quantum dots used for in vitro cellular labeling: role of QD surface ligand, delivery modality, cell type, and direct comparison to organic fluorophores. *Bioconjugate Chem. 24*, 1570−1583.
(15) Yuan, H., Miao, J., Du, Y.-Z., You, J., Hu, F.-Q., and Zeng, S. (2008) Cellular uptake of solid lipid nanoparticles and cytotoxicity of encapsulated paclitaxel in A549 cancer cells. *Int. J. Pharm. 348*, 137−145.
(16) Zhu, Y., Li, Z., Chen, M., Cooper, H. M., Lu, G. Q., and Xu, Z. P. (2012) Synthesis of robust sandwich-like SiO_2@CdTe@SiO_2 fluorescent nanoparticles for cellular imaging. *Chem. Mater. 24*, 421−423.
(17) Wang, Y. X., Xuan, S., Port, M., and Idee, J. M. (2013) Recent advances in superparamagnetic iron oxide nanoparticles for cellular imaging and targeted therapy research. *Curr. Pharm. Des. 19*, 6575−6593.
(18) Costantino, H. R., Firouzabadian, L., Hogeland, K., Wu, C., Beganski, C., Carrasquillo, K. G., Córdova, M., Griebenow, K., Zale, S. E., and Tracy, M. A. (2000) Protein spray-freeze drying. Effect of atomization conditions on particle size and stability. *Pharm. Res. 17*, 1374−1383.
(19) Yu, Z., Garcia, A. S., Johnston, K. P., and Williams, R. O. (2004) Spray freezing into liquid nitrogen for highly stable protein nanostructured microparticles. *Eur. J. Pharm. Biopharm. 58*, 529−537.
(20) Muhrer, G., and Mazzotti, M. (2003) Precipitation of lysozyme nanoparticles from dimethyl sulfoxide using carbon dioxide as antisolvent. *Biotechnol. Prog. 19*, 549−556.
(21) Lee, S. H., Heng, D., Ng, W. K., Chan, H.-K., and Tan, R. B. H. (2011) Nano spray drying: A novel method for preparing protein nanoparticles for protein therapy. *Int. J. Pharm. 403*, 192−200.
(22) Weber, C., Coester, C., Kreuter, J., and Langer, K. (2000) Desolvation process and surface characterisation of protein nanoparticles. *Int. J. Pharm. 184*, 91−102.
(23) Montalvo, B. L., Pacheco, Y., Sosa, B. A., Velez, D., Sanchez, G., and Greibenow, K. (2008) Formation of spherical protein nanoparticles without impacting protein integrity. *Nanotechnology 19*, 465103.
(24) Gulseren, I., Fang, Y., and Corredig, M. (2012) Zinc incorporation capacity of whey protein nanoparticles prepared with desolvation with ethanol. *Food Chem. 135*, 770−774.
(25) Aimi, M., Nemori, R., Miyashita, Y., and Yokoyama, H. (2009) Enzymatically crosslinked protein nanoparticles, U.S. Patent Appl. No. 2009/0004278 A1.
(26) Chattopadhyay, P., and Gupta, R. B. (2002) Protein nanoparticles formation by supercritical antisolvent with enhanced mass transfer. *AIChE J. 48*, 235−244.
(27) Kamat, S. V., Beckman, E. J., and Russell, A. J. (1995) Enzyme activity in supercritical fluids. *Crit. Rev. Biotechnol. 15*, 41−71.
(28) Sarkari, M., Darrat, I., and Knutson, B. L. (2003) CO_2 and fluorinated solvent-based technologies for protein microparticle precipitation from aqueous solutions. *Biotechnol. Prog. 19*, 448−454.
(29) Won, Y.-W., and Kim, Y.-H. (2008) Recombinant human gelatin nanoparticles as a protein drug carrier. *J. Controlled Release 127*, 154−161.
(30) Singh, R., Singh, S., and Lillard, J. W. (2008) Past, present, and future technologies for oral delivery of therapeutic proteins. *Eur. J. Pharm. Sci. 97*, 2497−2523.
(31) Hawkins, M. J., Soon-Shiong, P., and Desai, N. (2008) Protein nanoparticles as drug carriers in clinical medicine. *Adv. Drug Delivery Rev. 60*, 876−885.
(32) Pathak, Y., and Thassu, D. (2009) *Drug delivery nanoparticles formulation and characterization*; Informa Healthcare: New York.
(33) Elzoghby, A. O., Samy, W. M., and Elgindy, N. A. (2012) Albumin-based nanoparticles as potential controlled release drug delivery systems. *J. Controlled Release 157*, 168−182.
(34) Subia, B., and Kundu, S. C. (2012) Drug loading and release on tumor cells using silk fibroin-albumin nanoparticles as carriers. *Nanotechnology 24*, 035103 24, 1..
(35) de la Fuente, J. M., and Berry, C. C. (2005) Tat peptide as an efficient molecule to translocate gold nanoparticles into the cell nucleus. *Bioconj. Chem. 16*, 1176−1180.
(36) Khalil, I. A., Kogure, K., Akita, H., and Harashima, H. (2006) Uptake pathways and subsequent intracellular trafficking in nonviral gene delivery. *Pharmacol. Rev. 58*, 32−45.
(37) Popovic, Z., Liu, W., Chauhan, V. P., Lee, J., Wong, C., Greytak, A. B., Insin, N., Nocera, D. G., Fukumura, D., Jain, R. K., et al. (2010) A nanoparticle size series for in vivo fluorescence imaging. *Angew. Chem., Int. Ed. 49*, 8649−8652.
(38) Kim, K. R., Ahn, K. Y., Park, J. S., Lee, K. E., Jeon, H., and Lee, J. (2011) Lyophilization and enhanced stability of fluorescent protein nanoparticles. *Biochem. Biophys. Res. Commun. 408*, 225−229.
(39) Qin, W., Ding, D., Liu, J., Yuan, W. Z., Hu, Y., Liu, B., and Tang, B. Z. (2012) Biocompatible nanoparticles with aggregation-induced emission characteristics as far-red/near-infrared fluorescent bioprobes for in vitro and in vivo imaging applications. *Adv. Funct. Mater. 22*, 771−779.
(40) Bhirde, A. A., Patel, V., Gavard, J., Zhang, G., Sousa, A. A., Masedunskas, A., Leapman, R. D., Weigert, R., Gutkind, J. S., and Rusling, J. F. (2009) Targeted killing of cancer cells in vivo and in vitro with EGF-directed carbon nanotube-based drug delivery. *ACS Nano 3*, 307−316.
(41) Liang, M., Lin, I. C., Whittaker, M. R., Minchin, R. F., Monteiro, M. J., and Toth, I. (2010) Cellular uptake of densely packed polymer coatings on gold nanoparticles. *ACS Nano 4*, 403−413.
(42) Ryan, J. A., Overton, K. W., Speight, M. E., Oldenburg, C. N., Loo, L., Robarge, W., Franzen, S., and Feldheim, D. L. (2007) Cellular uptake of gold nanoparticles passivated with BSA-SV40 large T antigen conjugates. *Anal. Chem. 79*, 9150−9159.
(43) Mandal, D., Maran, A., Yaszemski, M. J., Bolander, M. E., and Sarkar, G. (2009) Cellular uptake of gold nanoparticles directly cross-linked with carrier peptides by osteosarcoma cells. *J. Mater. Sci., Mater. Med. 20*, 347−350.
(44) Nigen, M., Gaillard, C., Croguennec, T., Madec, M. N., and Bouhallab, S. (2010) Dynamic and supramolecular organization of alpha-lactalbumin/lysozyme microspheres: A microscopic study. *Biophys. Chem. 146*, 30−35.
(45) Hoffmann, C., Leroy-Dudal, J., Patel, S., Gallet, O., and Pauthe, E. (2008) Fluorescein isothiocyanate-labeled human plasma fibronectin in extracellular matrix remodeling. *Anal. Biochem. 372*, 62−71.

DOI: 10.1021/bc500621h
Bioconjugate Chem. 2015, 26, 396−404

(46) Pernodet, N., Maaloum, M., and Tinland, B. (1997) Pore size of agarose gels by atomic force microscopy. *Electrophoresis 18*, 55−58.
(47) Sheldon, R. A., Schoevaart, R., and Van Langen, L. M. (2005) Cross-linked enzyme aggregates (CLEAs): A novel and versatile method for enzyme immobilization (a review). *Biocatal. Biotransform. 23*, 141−147.
(48) Volk, T., Hensel, M., and Kox, W. J. (1997) Transient Ca2+ changes in endothelial cells induced by low doses of reactive oxygen species: role of hydrogen peroxide. *Mol. Cell. Biochem. 171*, 11−21.
(49) Waters, C. M., Savla, U., and Panos, R. J. (1997) KGF prevents hydrogen peroxide-induced increases in airway epithelial cell permeability. *Am. J. Physiol. 272*, L681−689.
(50) Nagai, H., and Totokuni, S. (2012) Differences and similarities between nanotubes and asbestos fibers during mesothelial carcinogenesis: Shedding light on fiber entry mechanism. *Cancer Sci. 103*, 1378−1390.
(51) Ruan, G., Agrawal, A., Marcus, A. I., and Nie, S. (2007) Imaging and tracking of Tat peptide-conjugated quantum dots in living cells: new insights into nanoparticle uptake, intracellular transport, and vesicle shedding. *J. Am. Chem. Soc. 129*, 14759−14766.
(52) Song, S., Liang, Z., Zhang, J., Wang, L., Li, G., and Fan, C. (2009) Gold-Nanoparticle-Based Multicolor Nanobeacons for Sequence-Specific DNA Analysis. *Angew. Chem., Int. Ed. 48*, 8670.
(53) Xu, H., Li, Q., Wang, L., He, Y., Shi, J., Tang, B., and Fan, C. (2014) Nanoscale optical probes for cellular imaging. *Chem. Soc. Rev. 43*, 2650−2661.
(54) Aiswal, A., Ghosh, S. S., and Chattopadhyay, A. (2012) One step synthesis of C-dots by microwave mediated caramelization of poly(ethylene glycol). *Chem. Commun. 48*, 407−409.
(55) Heller, D. A., Baik, S., Eurell, T. E., and Strano, M. S. (2005) Single-walled carbon nanotube spectroscopy in live cells: towards long-term labels and optical sensors. *Adv. Mater. 17*, 2793−279.
(56) Cheng, J., Fernando, K. A. S., Veca, L. M., Sun, Y.-P., Lamond, A. I., Lam, Y. W., and Cheng, S. H. (2008) Reversible accumulation of PEGylated single-walled carbon nanotubes in the mammalian nucleus. *ACS Nano 2*, 2085−2094.
(57) Tung, C. H., and Stein, S. (2000) Preparation and applications of peptide-oligonucleotide conjugates. *Bioconjugate Chem. 11*, 605−618.
(58) Pattammattel, A., Deshapriya, I. K., Chowdhury, R., and Kumar, C. V. (2013) Metal-enzyme frameworks: Role of metal ions in promoting the self-assembly on α-zirconium(IV) phosphate nanoplates. *Langmuir 29*, 2971−81.
(59) Nelson, D. R., and Huggins, A. K. (1974) Interference of 5-hydroxytryptamine in the assay of glucose by glucose oxidase: peroxidase:chromogen based methods. *Anal. Biochem. 59*, 46−53.
(60) Anderson, J., Byrne, T., Woelfel, K. J., Meany, J. E., Spyridis, G. T., and Pocker, Y. (1994) The hydrolysis of p-nitrophenyl acetate: a versatile reaction to study enzyme kinetics. *J. Chem. Educ. 71*, 715.
(61) Lee, J., Lee, D., Oh, E., Kim, J., Kim, Y. P., Jin, S., Kim, H. S., Hwang, Y., Kwak, J. H., Park, J. G., et al. (2005) Preparation of a magnetically switchable bio-electrocatalytic system employing cross-linked enzyme aggregates in magnetic mesocellular carbon foam. *Angew. Chem., Int. Ed. 117*, 7593−7598.

DOI: 10.1021/bc500621h
Bioconjugate Chem. 2015, 26, 396−404